Nanoscale

REVIEW

View Article Online
View Journal | View Issue

Cite this: *Nanoscale*, 2017, **9**, 6204

Recent progress in biomedical applications of persistent luminescence nanoparticles

Jie Wang, Qinqin Ma, Yingqian Wang, Haijing Shen and Quan Yuan *

Received 1st March 2017,
Accepted 7th April 2017

DOI: 10.1039/c7nr01488k

rsc.li/nanoscale

Persistent luminescence nanoparticles (PLNPs) are an emerging group of promising luminescent materials that can remain luminescent after the excitation ceases. In the past decade, PLNPs with intriguing optical properties have been developed and their applications in biomedicine have been widely studied. Due to the ultra-long decay time of persistent luminescence, autofluorescence interference in biosensing and bioimaging can be efficiently eliminated. Moreover, PLNPs can remain luminescent for hours, making them valuable in biotracing. Also, persistent luminescence imaging can guide cancer therapy with a high signal-to-noise ratio (SNR) and superior sensitivity. Briefly, PLNPs are demonstrated to be a newly-emerging class of functional materials with unprecedented advantages in biomedicine. In this review, we summarized recent advances in the preparation of PLNPs and the applications of PLNPs in biosensing, bioimaging and cancer therapy.

1. Introduction

Persistent luminescence refers to the phenomenon whereby luminescence lasts for several seconds to a few days after the excitation ceases.[1–3] This interesting phenomenon was discovered about a thousand years ago. For instance, some ancient Chinese paintings are visible in the dark.[3,4] The first documented description of persistent luminescence is at the beginning of the 17th century with the discovery of the famous Bologna Stone.[3,4] For many decades, the persistent luminescence phenomenon did not catch much attention from researchers, and ZnS:Cu^{2+},Co^{2+} with poor persistent luminescence served as the most widely used persistent phosphor for quite a long time.[3] In 1996, Matsuzawa *et al.* achieved a significant milestone in the development of persistent phosphors by developing the well-known $SrAl_2O_4$:Eu^{2+},Dy^{3+} phosphor that can give bright green emission for many hours after the stoppage of excitation.[2] The persistent luminescence in $SrAl_2O_4$:Eu^{2+},Dy^{3+} is more than 10 times brighter than that in ZnS:Cu^{2+},Co^{2+}. This inspiring discovery received enormous attention and many researchers started to search for different and more per-

Key Laboratory of Analytical Chemistry for Biology and Medicine (Ministry of Education), College of Chemistry and Molecular Sciences, Wuhan University, Wuhan, 430072, People's Republic of China. E-mail: yuanquan@whu.edu.cn

Jie Wang

Jie Wang received his B.S. from the School of Chemical Engineering and Pharmacy, Wuhan Institute of Technology in 2012. He is now pursuing his Ph.D. degree under the supervision of Prof. Quan Yuan at the Key Laboratory of Analytical Chemistry for Biology and Medicine (Ministry of Education), College of Chemistry and Molecular Sciences, Wuhan University. His research interests include the development of functional nanomaterials for biosensing and bioimaging.

Qinqin Ma

Qinqin Ma received her B.S. from the College of Chemistry and Molecular Sciences, Wuhan University in 2015. She is currently pursuing her master's degree under the supervision of Prof. Quan Yuan at the Key Laboratory of Analytical Chemistry for Biology and Medicine (Ministry of Education), College of Chemistry and Molecular Sciences, Wuhan University. Her research focuses on the controlled synthesis of novel luminescent nanomaterials for biomedical applications.

sistent phosphors. Since then, a large variety of persistent phosphors have been developed and they are widely used in traffic signs, emergency signage, watches and so on.[1,3,5–9]

In 2007, Chermont *et al.* reported their creative work about utilizing persistent luminescence nanoparticles (PLNPs) for bioimaging,[10] which opened a new door to the application of persistent phosphors. The PLNPs show unprecedented advantages in bioimaging because they possess the following two unique characteristics.[11,12] The most paramount one is that PLNPs can remain luminescent after the excitation ceases, which allows imaging without *in situ* excitation.[13] Therefore, interference from tissue autofluorescence is completely eliminated, and thus a superior signal-to-noise ratio (SNR) as well as significantly improved sensitivity can be achieved.[14,15] The second feature is that the persistent luminescence can last for a long time (even to several days), which makes PLNPs ideal for long-term bioimaging, such as cell-tracing.[16,17] Now there is increasing interest in the biomedical applications of PLNPs. Many research studies have been conducted to optimize the size, shape and dispersibility of PLNPs.[11,18,19] Different methods have also been proposed to enhance the persistent luminescence intensity and increase the decay time in PLNPs to improve imaging sensitivity in bioimaging.[14,20,21] Moreover, intriguing energy transfer processes are designed to obtain persistent luminescence in the near-infrared (NIR) region to enhance the tissue penetration capability of the persistent signal.[22] Some pioneering works have also been reported recently to explore the applications of PLNPs in cancer therapy.[23,24] In a word, great efforts have been made in the past two decades to promote the application of PLNPs in biomedicine.

With a deeper understanding of persistent luminescence and the rapid development of persistent phosphors, more and more advanced scientific applications based on persistent phosphors have been explored.[1] A number of excellent reviews emphasizing the synthesis of persistent phosphors and their applications have been published. For example, Qiu *et al.* recently made a very comprehensive summary about the synthetic methods, persistent luminescence mechanisms, characterization techniques, materials system, and the many applications of persistent phosphors.[1] Richard *et al.* introduced the persistent luminescence in Cr^{3+} doped spinels and their applications in *in vivo* bioimaging.[25] They further provided a comprehensive summary about the bioimaging applications of chemically engineered persistent luminescence nanoprobes.[26] Zhuang *et al.* summarized the red to near-infrared persistent phosphors activated by transition metals (Cr^{3+} or Mn^{2+}).[12] Eeckhout *et al.* systematically summarized the important classes of known persistent luminescence in Eu^{2+} doped phosphors.[3] However, the biomedical applications of PLNPs are seldom summarized. The aim of this review is to provide a summary of the recent achievements in biosensing, bioimaging and cancer therapy applications of PLNPs.

2. Brief description of the persistent luminescence mechanism

In order to gain a better understanding of persistent luminescence and its related biomedical application, it is necessary to give a brief introduction about the luminescence mechanism. This section only presents a general idea about the persistent luminescence mechanism. The detained mechanism of persistent luminescence can be found in some previously published works.[1,3,27]

It is generally accepted that two kinds of active centers are mainly responsible for the generation of persistent luminescence: traps and emitters.[3,26] In persistent phosphors, intrinsic crystal defects and codopants can serve as the traps, which are just a few electron volts (eV) below the conduction bands of the host material.[27,28] The emitters are usually lanthanide or transition metal ions. The formation of persistent luminescence can be divided into four consecutive processes: the generation of charge carriers, trapping of charge carriers, release of the trapped charge carriers, and recombination of the released charge carriers to produce emission.[29,30] Qiu *et al.* have provided a brief illustration to describe the above four processes,[31] as shown in Fig. 1. Upon

Yingqian Wang

Yingqian Wang obtained her B.S. from the College of Chemistry and Chemical Engineering, Hunan University in 2015. She is currently pursuing her master's study under the supervision of Prof. Quan Yuan at the Key Laboratory of Analytical Chemistry for Biology and Medicine (Ministry of Education), College of Chemistry and Molecular Sciences, Wuhan University. She is interested in the design of DNA-based nanomaterials and exploring their potential biomedical applications.

Haijing Shen

Haijing Shen obtained her B.S. from the College of Chemistry and Molecular Engineering, Zhengzhou University in 2014. She is currently a PhD candidate under the supervision of Prof. Quan Yuan at the Key Laboratory of Analytical Chemistry for Biology and Medicine (Ministry of Education), College of Chemistry and Molecular Sciences, Wuhan University. Her research interest is in developing multifunctional nanomaterials for biomedical applications.

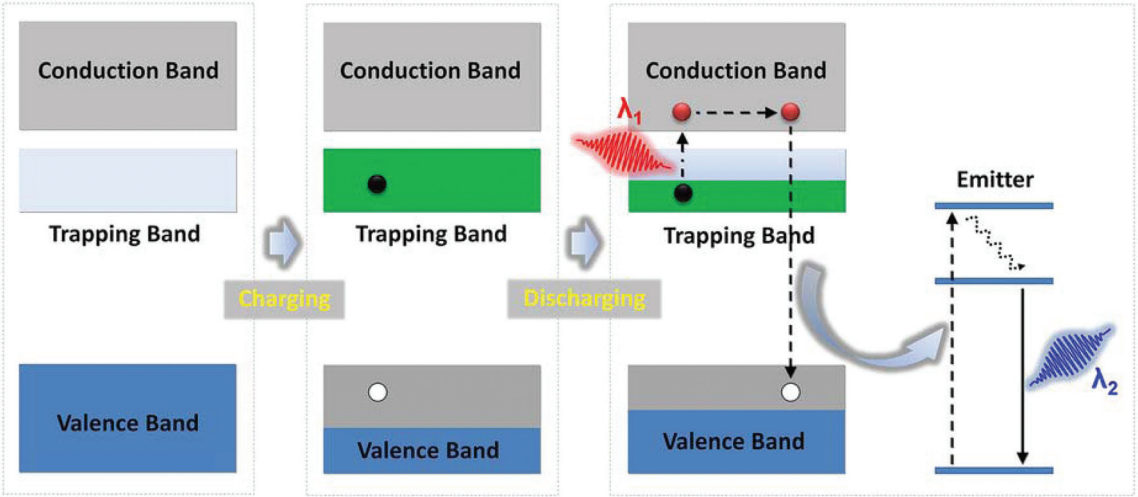

Fig. 1 Brief description of the persistent luminescence mechanism. (Reprinted with permission from ref. 31. Copyright 2014 Nature Publishing Group.)

efficient excitation (electron beam, X rays and UV light), charge carriers such as electrons and holes are generated. Then the charge carriers are captured by traps in the crystal, and they can be stored within traps for a long time. These two processes are also called charging of the material. Under thermal or optical stimulations, the captured charge carriers escape from traps and further recombine with the emitters to produce the so-called persistent luminescence.

3. Preparation of PLNPs

As we just mentioned, traps are one of the main active centers in persistent phosphors and intrinsic crystal defects are an important kind of trap. A high sintering temperature is generally beneficial for the formation of intrinsic defects, indicating that high temperature treatment is usually involved in the preparation of persistent phosphors.[1,32] High temperature annealing generally produces persistent phosphors with large sizes and poor dispersibility. However, the biomedical applications require PLNPs with small sizes, good monodispersity and easy modification. In the past few decades, several post treatment methods have been proposed to solve the problems associated with high temperature annealing.[11,33] Moreover, a few pioneering studies have reported the direct synthesis of PLNPs with small sizes and good dispersibility with the reaction proceeding under a relatively low temperature.[17,34,35] This section will introduce recent advances in the preparation of PLNPs. As a previous review has already summarized the many kinds of methods (solid state reaction, sol–gel procedure, hydrothermal route and so on) for the preparation of persistent phosphors,[1] it is unnecessary to list these methods again. Therefore, the many synthesis methods are simply divided into two categories, that is, the top-down manner and bottom-up manner.

Quan Yuan

Professor Quan Yuan is currently a full professor at the College of Chemistry and Molecular Sciences at Wuhan University. She received her B.S. degree from the College of Chemistry and Molecular Sciences, Wuhan University in 2004. She obtained her Ph.D. degree from the College of Chemistry and Molecular Engineering, Peking University in 2009. Afterward, she continued her postdoctoral research on DNA molecules with Prof. Weihong Tan at University of Florida. In 2012, she joined the College of Chemistry and Molecular Sciences, Wuhan University as a full professor. Her research interests include the controlled synthesis of functional nanomaterials and investigating their corresponding biomedical applications.

3.1 Top-down manner

The most conventional method for the synthesis of persistent phosphors is a solid-state reaction which occurs between powders in the solid state under high temperature calcination.[1–3,36] The sol–gel process is also widely employed in the preparation of persistent phosphors.[1,10] Generally, this process involves the combination of precursors (metal salts or alkoxide), chelating ligands and cross-linking agents to prepare a polymeric resin. Then the obtained polymeric resin is calcined under high temperature to form compounds with persistent luminescence. The persistent phosphors prepared by the solid-state reaction or sol–gel method are generally bulk compounds, and post physical treatments such as grinding are

usually required to break down the bulk phosphors into nanophosphors.[10] Many kinds of PLNPs have been prepared with the top-down manner and they have been widely used in bioimaging.[10,14,37,38] As a high temperature treatment is involved, the obtained PLNPs usually possess strong and durable persistent luminescence.

In 2007, Chermont *et al.* reported the application of PLNPs in bioimaging for the first time.[10] The employed $Ca_{0.2}Zn_{0.9}Mg_{0.9}Si_2O_6:Eu^{2+},Dy^{3+},Mn^{2+}$ PLNPs were prepared with the sol–gel approach. Briefly, metal salt precursors and tetraethoxysilane were reacted at 70 °C to induce the sol-to-gel transition, and the dried gel was further fired at 1050 °C for 10 h in a weakly reductive atmosphere. The resulting persistent phosphors were ground with a mortar, and the smallest particles were isolated by selective sedimentation. The obtained PLNPs were further treated with NaOH solution to introduce hydroxyl groups to their surface for the subsequent bio-conjugation. The prepared PLNPs exhibited size distribution in the range of 50 to 100 nm, and the persistent luminescence was in the NIR region with the maximum intensity at about 690 nm. The persistent luminescence in the PLNPs was recorded with a photon-counting system based on a cooled GaAs intensified charge-coupled device camera. The authors showed that the persistent luminescence was detectable for over 24 h in the dark (Fig. 2).

Since then, many other kinds of PLNPs were prepared and widely employed in biomedicine.[39,40] Richard *et al.* reported the preparation of $ZnGa_2O_4:Cr^{3+}$ PLNPs with the hydrothermal method followed by sintering in air at 750 °C for 5 h.[11] Basic wet grinding was further applied to the calcined phosphor, and PLNPs with the desired size were collected by selective sedimentation. The PLNPs were functionalized with polyethylene glycol for bioimaging applications. The $ZnGa_2O_4:Cr^{3+}$ PLNPs show size distribution in the range of 20–60 nm, and the hydrodynamic diameter of the PLNPs is about 80 nm. Yan *et al.* reported the synthesis of $Zn_{2.94}Ga_{1.96}Ge_2O_{10}:Cr^{3+},Pr^{3+}$ PLNPs based on a citrate sol–gel method in combination with subsequent calcination in air and wet grinding.[15] The PLNPs show a diameter of about 48.7 nm. It is worth mentioning that they found that the persistent luminescence intensity and decay time in the PLNPs strongly depended on the calcination temperature. An increase of the calcination temperature can lead to an increase of the persistent luminescence intensity and decay time. Solid state reaction was also widely employed in the preparation of PLNPs. For example, Maldiney *et al.* reported the synthesis of $Ca_2Si_5N_8:Eu^{2+},Tm^{3+}$ PLNPs using solid state reaction followed by pulsed laser ablation.[41] The stoichiometric amounts of precursors were mixed together and then sintered at 1300 °C for 1 h under a reducing atmosphere. The final PLNPs were obtained with a pulsed laser ablation technique in solution. With this method, the authors successfully prepared small PLNPs with diameters in the range of 3–5 nm.

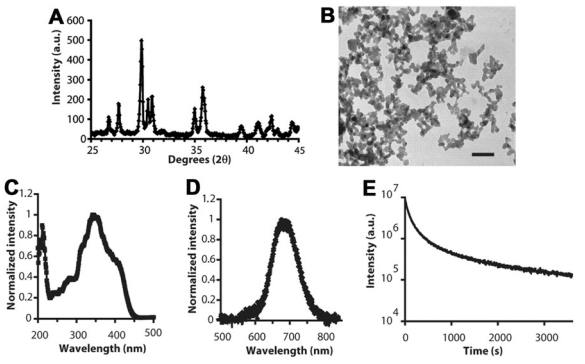

Fig. 2 Physical characterization of the $Ca_{0.2}Zn_{0.9}Mg_{0.9}Si_2O_6:Eu^{2+},Dy^{3+},Mn^{2+}$ PLNPs. X-ray powder diffraction (XRD) spectrum (A), transmission electron microscopy (TEM) image (B), photoexcitation spectrum (C), persistent luminescence (D) and decay (E) spectra of the PLNPs. (Reprinted with permission from ref. 10. Copyright 2007 National Academy of Sciences.)

3.2 Bottom-up manner

Compared to the top-down approach, the bottom-up manner shows obvious advantages for the preparation of nanomaterials in terms of the morphology and homogeneity control. Recently, new synthesis strategies have been proposed for the preparation of PLNPs with a controllable size, uniform shape and effective surface functionalization.[17,42]

Hydrothermal synthesis refers to the preparation of nanomaterials by treating the precursors in a sealed heated solution above ambient temperature and pressure.[43,44] This method enables the synthesis of highly crystalline nanomaterials under relatively mild conditions. Moreover, the reaction parameters of a hydrothermal reaction, such as the pH value, reaction time and reaction temperature, can be easily controlled to tune the properties of the nanomaterials.[45] The most successful example for the hydrothermal synthesis of PLNPs was demonstrated by Han *et al.* in 2015.[18] The proposed solution-phase reaction procedure for the preparation of $ZnGa_2O_4:Cr^{3+}$ PLNPs is outlined in Fig. 3A. The precursors are simply mixed together and subjected to hydrothermal treatment at 220 °C for 10 h. The whole synthesis process is very simple and easy to perform. The obtained $ZnGa_2O_4:Cr^{3+}$ PLNPs display a narrow size distribution with an average size of about 8 nm. Moreover, the PLNPs can readily disperse in water to form a transparent colloidal solution, and the solution is stable for more than one month (Fig. 3F and G). Such stable and monodisperse attributes are premises for the further surface functionalization of the PLNPs. A step further, Zhang *et al.* recently reported the one-step hydrothermal synthesis of amino-functionalized $ZnGa_2O_4:Cr^{3+},Eu^{3+}$ PLNPs.[46] This novel approach is based on a synthetic strategy in which ethylenediamine serves as both the surfactant ligand to control the nanocrystal size and the reactant to form surface amino groups under hydrothermal conditions. The obtained $ZnGa_2O_4:Cr^{3+},Eu^{3+}$ PLNPs showed a uniform shape with an average size of 5–7 nm. Moreover, the PLNPs can be easily functionalized with biomolecules for further applications due to the presence of surface amino groups. Mao *et al.* developed a novel biphasic

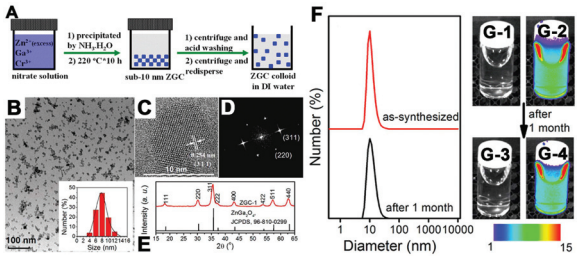

Fig. 3 (A) Schematic illustration of the synthesis of $ZnGa_2O_4:Cr^{3+}$ PLNPs. TEM image (B), high-resolution TEM image (C), selected area's electron diffraction (D) and XRD measurement (E) of the PLNPs. (F) Dynamic light scattering (DLS) patterns of the PLNPs in water before and after storage for 1 month. (G-1, G-3) Bright field and (G-2, G-4) corresponding luminescence pictures of PLNPs in water. (Reprinted with permission from ref. 18. Copyright 2015 American Chemical Society.)

hydrothermal approach for the synthesis of $ZnGa_2O_4:Cr^{3+}$ PLNPs with a controlled size through the hydrolysis of the corresponding inorganic salts in a water–toluene system. The obtained PLNPs are nearly monodisperse with sizes of about 6.1 nm.[34] Similarly, Manam *et al.* also prepared $MgGa_2O_4:Cr^{3+}$ PLNPs with the size in the 10–70 nm range by the hydrothermal method.[47] The hydrothermal method holds great potential in the preparation of PLNPs by providing good morphology/homogeneity control and excellent dispersibility. However, the present success is only limited to gallate-based PLNPs. The application of the hydrothermal method in the preparation of other kinds of PLNPs needs to be further explored. Moreover, the relatively low temperature involved in hydrothermal synthesis may lead to a short persistent luminescence in the obtained PLNPs.

The template method is another well-developed synthesis strategy to prepare nanomaterials. Many researchers have reported the preparation of PLNPs by utilizing mesoporous silica nanoparticles (MSNs) as the template.[17,42,48–50] The template method developed by Zhang *et al.* to prepare PLNPs with a narrow size distribution is illustrated in Fig. 4A.[42] Metal ions

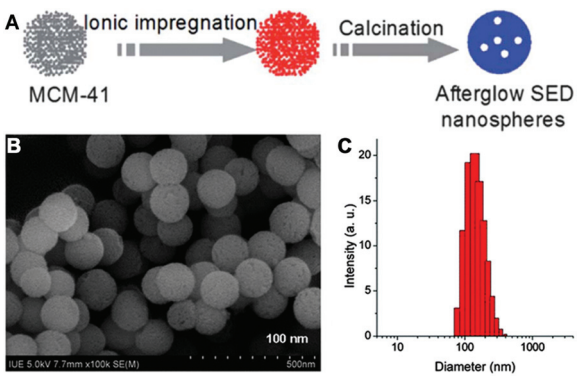

Fig. 4 (A) Synthesis of the $SiO_2/SrMgSi_2O_6:Eu^{2+},Dy^{3+}$ PLNPs. Scanning electron microscopy (SEM) image (B) and DLS (C) pattern of the PLNPs. (Reprinted with permission from ref. 42. Copyright 2012 Royal Society of Chemistry.)

making up the PLNPs are impregnated into the mesopores of MSNs, and the obtained MSNs are further annealed under high temperature to form persistent PLNPs with a narrow size distribution. They have successfully utilized this method for the preparation of many kinds of PLNPs, such as $SiO_2/SrMgSi_2O_6:Eu^{2+},Dy^{3+}$,[42] $SiO_2/CaMgSi_2O_6:Eu^{2+},Pr^{3+},Mn^{2+}$,[48] $SiO_2/CaTiO_3:Pr^{3+}$,[51] and $SiO_2/Zn_{1.1}Ga_{1.8}Ge_{0.1}O_4:Cr^{3+},Eu^{3+}$.[52] All of the obtained PLNPs show regular spherical morphologies and narrow size distributions. The preparation of other PLNPs with this template method was also reported, such as $SiO_2/ZnGa_2O_4:Cr^{3+}$, and $SiO_2/SrAl_2O_4:Eu^{2+},Dy^{3+}$.[48] Moreover, Zhang *et al.* further promoted this method by depositing PLNPs in the mesoporous shell of core–shell nanoparticles to prepare multifunctional PLNPs.[53] For instance, Gd_2O_3 nanoparticles are coated with ordered mesoporous silica, and a $CaTiO_3:Pr^{3+}$ persistent phosphor is further deposited into the mesopores to form the $Gd_2O_3@mSiO_2@CaTiO_3:Pr^{3+}$ multifunctional PLNPs. The obtained PLNPs hold typical ordered mesoporous characteristics and a spherical morphology with a narrow size distribution. Similarly, the preparation of $Gd_2O_3@mSiO_2/ZnGa_2O_4:Cr^{3+},Bi^{3+}$ multifunctional PLNPs was recently reported by another research group.[54] The template method is a potent and easily-performed approach to prepare different kinds of PLNPs. However, the morphology and size of such hybrid PLNPs are restricted by the employed MSNs. Also, high-temperature calcination leads to the loss of surface functional groups, which may result in poor dispersibility of the hybrid PLNPs.

In addition to hydrothermal synthesis and the template method, other bottom-up approaches have also been developed for the preparation of PLNPs.[55–57] Lalatonne *et al.* described a facile non-aqueous sol–gel method assisted with microwave irradiation for the preparation of $ZnGa_2O_4:Cr^{3+}$ PLNPs with an average diameter of 6 nm.[35] The synthesis reaction was performed at moderate temperature and pressure to obtain very small PLNPs with good dispersibility. Moreover, the proposed microwave heating offers a reduction of the reaction time to 30 min, which is much shorter than that of the hydrothermal heating (10–48 h). Liu *et al.* have reported the direct synthesis of $Y_2O_2S:Eu^{3+},Mg^{2+},Ti^{4+}$ PLNPs by using $Y(OH)_3$ as the precursor.[58] The size of the prepared PLNPs ranges from 30 to 50 nm, and the PLNPs show uniform sizes and a well-dispersed distribution.

The preparation of PLNPs with the bottom-up method is still at the early stage. Until now, only limited methods have been developed and the reported kinds of PLNPs are also far from reaching the requirements in biomedical applications. The controlled synthesis of PLNPs with a highly tunable size, strong persistent luminescence intensity and long decay time to fulfil the different desires in biomedicine has not been reported at present.

4. Biosensing based on PLNPs

Time-resolved luminescent biosensing is one of the most efficient methods in eliminating autofluorescence interference.[59–63]

However, this technique usually involves complicated and expensive instruments. The PLNPs can avoid autofluorescence in a similar but easy-to-perform manner due to their super long persistent time. In this section, the pioneering work in exploring the biosensing applications of PLNPs will be introduced.

Yan *et al.* reported the autofluorescence-free detection of α-fetoprotein (AFP) with PLNPs.[38] AFP is a serum biomarker of hepatocellular carcinoma, and serum AFP often increases under conditions such as rapid liver cancer cell growth and cirrhosis.[64] The detection of serum AFP can lead to the early diagnosis of hepatocellular carcinoma. Yan *et al.* designed a fluorescence resonance energy transfer (FRET) inhibition assay between $Ca_{1.86}Mg_{0.14}ZnSi_2O_7:Eu^{2+},Dy^{3+}$ PLNPs and antibody-coated gold nanoparticles for the detection of AFP in serum samples and in cancer cells. The FRET inhibition assay for AFP detection is illustrated in Fig. 5A. The FRET probe is pre-charged with UV light, thus autofluorescence interference and scattering light associated with *in situ* excitation are effectively eliminated. The FRET inhibition probe was successfully utilized in the detection of serum AFP and in the imaging of AFP in Bel-7402 cells (Fig. 5B). Tang *et al.* also constructed a novel FRET probe for the detection of ascorbic acid (AA) in living cells and in mice based on the specific reaction of cobalt oxyhydroxide (CoOOH) and AA.[65] The biosensing principle is illustrated in Fig. 5C. Briefly, $Sr_2MgSi_2O_7:Eu^{2+},Dy^{3+}$ PLNPs are modified with CoOOH and the persistent luminescence is efficiently quenched. In the presence of AA, CoOOH is reduced to Co^{2+} and the persistent luminescence of PLNPs is restored. The probe showed an instantaneous response to AA and a good linear correlation between the persistent luminescence intensity and the AA concentrations was observed. Moreover, *in vivo* detection of AA without *in situ* excitation was achieved due to the long decay time of the persistent luminescence, which allows the removal of autofluorescence and light scattering from biological matrixes (Fig. 5D). Tang *et al.* further promoted the application of this biosensing method for the detection of glutathione in living cells and *in vivo* by using MnO_2-modified PLNPs.[66] Other research groups also reported autofluorescence-free biosensing with PLNPs. Such probes provide an effective platform for monitoring and imaging reactive species both *in vitro* and *in vivo*.[50,67,68]

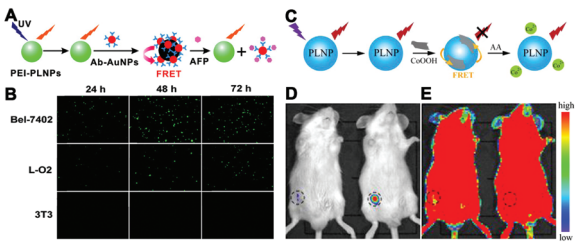

Fig. 5 (A) Schematic illustration of the FRET inhibition assay for AFP detection. (B) Fluorescence images of Bel-7402, L-O2, and 3T3 cells stained with the FRET inhibition probe after the cells had been cultured for 22, 46, and 70 h, respectively. (Reprinted with permission from ref. 38. Copyright 2011 American Chemical Society.) (C) Schematic illustration of the detection of AA with CoOOH-modified PLNPs. (D) Persistent luminescence image of mice treated with saline and a PLNP-based probe (left) and mice treated with AA and a PLNP-based probe (right). (E) Photoluminescence image of the same mice in (D) using 420 nm light excitation. (Reprinted with permission from ref. 65. Copyright 2014 American Chemical Society.)

The above studies are about the applications of PLNPs in homogeneous biosensing. The following example is of heterogeneous biosensing based on PLNPs. Immunochromatographic lateral flow assay is one of the most promising point-of-care methods for biosensing. Background fluorescence at the wavelengths of the reporter's emission may limit the sensitivity of lateral flow assays. Willson *et al.* employed PLNPs as the reporter to eliminate background fluorescence interference.[69] The $SrAl_2O_4:Eu^{2+},Dy^{3+}$ PLNPs were functionalized with NeutrAvidin and biotinylated lysozyme was employed as the analyte. The lysozyme was firstly captured by an antibody immobilized within the test strips, then the NeutrAvidin PLNPs were added to label the lysozyme by making use of the strong binding affinity between NeutrAvidin and biotin. The method achieved a detection limit of below 100 pg mL^{-1}, which was approximately an order of magnitude more sensitive than colloidal gold. This study shows that PLNPs are a promising reporter for lateral flow assay and they can potentially lead to more sensitive point-of-care tests.

5. Bioimaging based on PLNPs

Bioimaging has become an indispensable tool in modern biology and medicine because it enables researchers to decipher the behavior of biological systems in their native contexts at the molecular level.[70–72] In recent decades, the rapid development of bioimaging has put forward higher requirements for imaging probes in terms of sensitivity and stability.[73–75] The special advantages of PLNPs in eliminating tissue autofluorescence in bioimaging have already been clearly demonstrated, and growing interest in improving the bioimaging performance of PLNPs has been ignited. In this section, the multiple bioimaging applications of PLNPs will be introduced.

5.1 Bioimaging with UV light charged PLNPs

As we mentioned in section 2, high energy excitation sources such as an electron beam, X-rays and UV light are usually employed for the efficient generation of charge carriers.[1] It is well-known that such excitation sources can cause serious damage to biological tissues, thus they cannot be used for the *in vivo* activation of the injected PLNPs. For this reason, the first generation of a PLNP-based bioimaging probe needs to be charged prior to injection.

Chermont *et al.* carried out the preparation of the $Ca_{0.2}Zn_{0.9}Mg_{0.9}Si_2O_6:Eu^{2+},Dy^{3+},Mn^{2+}$ PLNPs and explored their capability in removing autofluorescence originating from *in situ* excitation for the first time.[10] Their bioimaging strategy is shown in Fig. 6A. The PLNP solution is pre-charged with UV light and then injected into mice. The persistent luminescence signal from the injected PLNPs is detected without *in situ* exci-

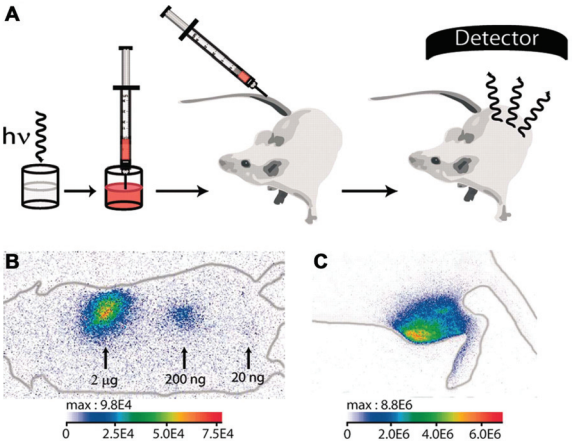

Fig. 6 (A) Schematic illustration of *in vivo* bioimaging with the UV lamp pre-charged $Ca_{0.2}Zn_{0.9}Mg_{0.9}Si_2O_6:Eu^{2+},Dy^{3+},Mn^{2+}$ PLNPs. (B) Persistent luminescence images of a mouse injected with PLNPs with different doses at different sites. The acquisition was performed during 2 min after injection. (C) Image of an intramuscular injection (200 μg) corresponding to a 90 s acquisition. (Reprinted with permission from ref. 10. Copyright 2007 National Academy of Sciences.)

tation. The authors showed that as low as 20 ng of injected PLNPs can produce a detectable signal with a good SNR of 5 (Fig. 6B). Also, the PLNPs displayed good performance in deep-tissue imaging. The PLNP solution was intramuscularly injected into a mouse, and the signal was clearly detectable in the tibial cranial muscle (Fig. 6C). Furthermore, optical imaging of mice injected with 1 mg of differently charged PLNPs was performed. The biodistribution of the PLNPs in mice was clearly visualized due to the superior SNR, and the results suggested that the biodistribution of PLNPs depended on the surface charge of PLNPs. The PLNPs were also successfully utilized for *in vivo* targeted tumor imaging. Richard *et al.* reported the functionalization of UV-charged PLNPs with targeting molecules for the specific recognition of the target cell lines.[76,77] Due to the absence of *in situ* excitation, the developed bio-functionalized PLNPs hold good potential to be used as sensitive probes for targeted cancer imaging in the future. The above works clearly proved the special advantages of PLNPs in eliminating background signal interference originating from *in situ* excitation.

A lot of PLNPs with other chemical compositions have also been developed for bioimaging applications. Yan *et al.* synthesized a kind of $Zn_{2.94}Ga_{1.96}Ge_2O_{10}:Cr^{3+},Pr^{3+}$ PLNP with super long persistent luminescence (4360 h) for *in vivo* bioimaging.[15] The developed PLNPs showed good promise in eliminating tissue autofluorescence and in long-term bioimaging. The authors further modified the PLNPs with Arg-Gly-Asp (RGD) peptide for targeted tumor imaging. The RGD-PLNPs showed improved tumor-specific accumulation capability than the PEG-PLNPs due to the high affinity of RGD towards integrin αvβ3 on tumor vasculature. Many other research groups also conducted exciting studies on *in vivo* bioimaging with pre-charged PLNPs.[37]

5.2 Bioimaging with visible light charged PLNPs

In 2012, Pan *et al.* reported a novel persistent phosphor $Zn_3Ga_2Ge_2O_{10}:Cr^{3+}$, and they demonstrated that the phosphor can be directly charged by sunlight under different outdoor conditions.[36] Richard *et al.* further introduced the new generation of $ZnGa_2O_4:Cr^{3+}$ PLNP-based probes whose persistent luminescence could be directly charged *in vivo* by incident light with deep penetration and low energy.[11] The photoluminescence excitation spectrum of $ZnGa_2O_4:Cr^{3+}$ shows two important regions in the visible region covering 425–570 nm due to the d–d transitions of the Cr^{3+} ion (Fig. 7A). The mechanism under the visible light activated persistent luminescence in $ZnGa_2O_4:Cr^{3+}$ is associated with the antisite defects around the Cr^{3+} ion, which was discussed in detail in previously published papers.[78,79] In this case, $ZnGa_2O_4:Cr^{3+}$ PLNPs were directly injected into mice without preliminary activation (Fig. 7B). The authors demonstrated that the injected PLNPs can be efficiently activated with an orange/red LED source (Fig. 7E). Such a simple excitation strategy with visible light was sufficient to activate the persistent luminescence in the injected PLNPs. This breakthrough in the development of PLNP-based probes for *in vivo* optical imaging allows the convenient recovery of the persistent luminescence, whenever required, which makes long-term *in vivo* bioimaging within reach. Many other types of Cr^{3+} doped gallate or gallogermanate PLNPs with *in vivo* activable persistent luminescence were further developed for bioimaging. For instance, Yan *et al.* have explored the application of Cr^{3+} doped gallate PLNPs in the long-term tracking of adipose-derived stem cells

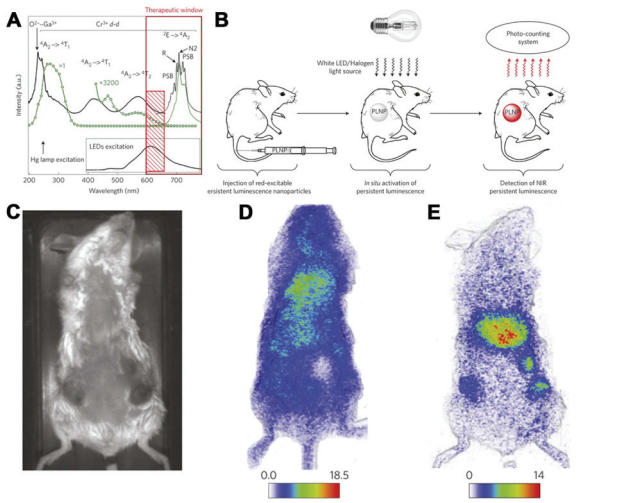

Fig. 7 (A) Excitation (black solid line) and emission (black dotted line) spectra of the $ZnGa_2O_4:Cr^{3+}$ PLNPs. (B) Schematic representation of *in vivo* imaging after *in situ* activation of PLNPs. (C) Optical image of a tumour-bearing mouse. (D) Persistent luminescence image of the mouse after injection with UV light pre-charged PLNPs. The image was acquired after 2 h of injection. (E) Persistent luminescence image of the mouse after the LED illumination. (Reprinted with permission from ref. 11. Copyright 2014 Nature Publishing Group.)

and long-term orally administered bioimaging, showing the broad application of the PLNPs in diagnosis and therapy.[80]

In addition to Cr^{3+} doped gallate/gallogermanate PLNPs, Zhang *et al.* showed that $SrAl_2O_4$:Eu^{2+},Dy^{3+} PLNPs can also be *in vivo* activated by visible light.[33] The excitation spectra of the $SrAl_2O_4$:Eu^{2+},Dy^{3+} PLNPs are quite broad and cover the UV to visible (400–470 nm) region, which is the basis of visible light activated persistent luminescence. The authors demonstrated that intense persistent luminescence of the injected PLNPs can be efficiently regenerated by a white-light LED lamp (400–475 nm) excitation, making it possible to detect the persistent luminescence signal over several days.

The second generation of PLNPs makes it possible to regenerate intense persistent luminescence *in vivo* whenever desired, which can significantly promote the applications of PLNPs in the long-term monitoring of molecular or cellular networks. However, PLNPs that can be directly charged by visible light are still limited at present.

5.3 Bioimaging with photostimulated PLNPs

Although PLNPs that can be charged by visible light are limited, researchers have found that persistent luminescence in many exhausted PLNPs can be regenerated under visible or NIR stimulation.[32,81–83] The mechanism of photostimulated persistent luminescence is described as follows. As we described in section 2, trapping is one of the most important factors for the generation of persistent luminescence. The persistent luminescence of PLNPs depends strongly on the amounts and types of traps. Generally, there are shallow traps and deep traps in PLNPs. Charge carriers in shallow traps can escape at physiological temperature and combine with the emitters to produce persistent luminescence. But if the trap is too deep, the charge carriers cannot escape and no persistent luminescence can be observed at physiological temperature. Researchers found that under visible or NIR light stimulations, the charge carriers can escape from deep traps to produce persistent luminescence.[83] Therefore, if persistent luminescence of the injected PLNPs exhausts, photostimulation can regenerate the luminescence signal for many times. This section focuses on the bioimaging applications of photostimulated PLNPs.

Pan *et al.* reported the photostimulable NIR persistent luminescence in $LiGa_5O_8$:Cr^{3+} PLNPs for ultrasensitive and longitudinal deep-tissue bioimaging.[83,84] They showed that white LED illumination can efficiently recover the persistent luminescence in $LiGa_5O_8$:Cr^{3+} PLNPs, which can be ascribed to the transfer of charge carriers from deep traps to shallow traps under photostimulation.[83] The PLNPs were pre-charged by ultraviolet light and further injected into mice. The PLNPs in deep tissue can be repeatedly stimulated *in vivo* for more than 20 times by short-illumination with a white LED, which expanded the tracking window from several hours to more than 10 days. They further performed a cell tracking study by intravenously injecting PLNP-labeled RAW264.7 cells into 4T1 tumor models, and the cell migration was successfully monitored over 3 days with white LED stimulation.

Compared to visible light, the NIR light shows deeper tissue penetration, which is more suitable for deep tissue bioimaging. The stimulation of persistent luminescence with NIR light for bioimaging is also widely studied. Qiu *et al.* used $Zn_3Ga_2Ge_2O_{10}$:Cr^{3+} PLNPs for deep tissue bioimaging with NIR LED (980 nm and 940 nm) stimulation.[31] The PLNP dispersion was injected into pork tissue at various injection depths. The injected PLNPs were further charged *ex situ* with a xenon short-arc lamp and *in situ* with X-ray, respectively. A strong luminescence signal was observed in both cases, and the persistent luminescence in the injected PLNPs was successfully recovered with the NIR LED stimulation (Fig. 8). Many other research groups have also reported the usage of NIR light stimulated persistent luminescence for bioimaging. Viana *et al.* probed the mechanism of photostimulated persistent luminescence in $ZnGa_2O_4$:Cr^{3+} PLNPs and further successfully utilized the PLNPs for the *in vivo* optical imaging of small animals with NIR stimulation.[81] Zhuang *et al.* reported the photostimulated persistent luminescence in a series of Zn$(Ga_{1-x}Al_x)_2O_4$:Cr^{3+},Bi^{3+} red PLNPs,[32] which could serve as promising probes for *in vivo* imaging systems. In addition to the above mentioned gallate-based PLNPs, photostimulated persistent luminescence is also observed in many other types of persistent phosphors, such as CaS:Eu^{2+},Dy^{3+},[82,85] Sr_2SiO_4:Eu^{2+},R^{3+} (R = Tm, Gd)[86] and $CaAl_2O_4$:Eu^{2+},R^{3+} (R = Nd, Dy, Tm).[87] These photostimulated persistent phosphors can provide new tools for long-term *in vivo* imaging.

As we introduced in the previous section, $ZnGa_2O4$:Cr^{3+} can be directly activated with orange/red light. Zhang *et al.* further combined the 650 nm visible-light-charged persistent luminescence in $ZnGa_2O_4$:Cr^{3+},Eu^{3+} PLNPs with 808 nm NIR photostimulation for targeted tumor imaging.[46] The PLNPs were functionalized with folic acid and pre-charged with UV light. Then the activated PLNPs were injected into H22 tumor-bearing mice *via* the tail vein. A SNR of 3.0 was still obtained after 10 min of decay, and the persistent luminescence was efficiently regenerated with 650 nm light excitation. After the regener-

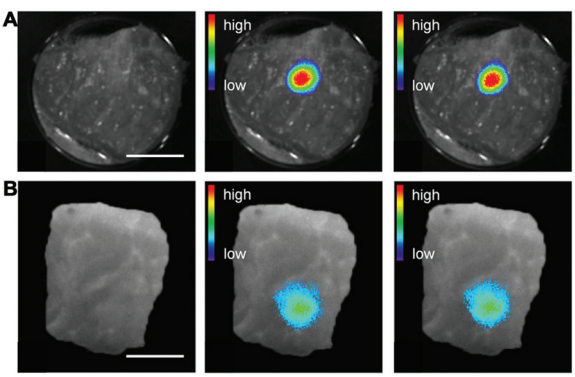

Fig. 8 (A) The application of *ex situ* optical charging (middle) and NIR photostimulation (right) for pork tissue imaging. (B) The application of X-ray *in situ* charging (middle) and NIR photostimulation (right) for pork tissue imaging. Scale bars are 15 mm. (Reprinted with permission from ref. 31. Copyright 2014 Nature Publishing Group.)

ated luminescence signal disappeared completely, tumor imaging with a high SNR (4.0) can be easily obtained under *in situ* stimulation with 808 nm light. Long-term and high SNR *in vivo* tumor-targeting imaging was also successfully achieved using 650 nm *in situ* excitation and 808 nm photostimulation.

5.4 Bioimaging with NIR-emitting PLNPs

Although the imaging sensitivity is mainly determined by the intensity of persistent luminescence in PLNP-based probes, an increase of the tissue penetration depth of the emission signal can also increase the imaging sensitivity. The penetration depth of light is significantly related to the absorption and scattering properties of biological tissues. Generally speaking, there are three tissue transparency windows in the NIR region: NIR-I, 650–950 nm; NIR-II, 1000–1350 nm; NIR-III, 1500–1800 nm.[88–90] The light absorption of tissue is at a minimum in the NIR region, which ensures deep tissue penetration. This section introduces the recently developed persistent phosphors with emission in the above three NIR windows.

The PLNPs with persistent luminescence in the NIR-I window primarily employ either Mn^{2+} or Cr^{3+} as one of the dopant/co-dopant ions. As we mentioned above, Chermont *et al.* showed that Mn^{2+} co-doped $Ca_{0.2}Zn_{0.9}Mg_{0.9}Si_2O_6:Eu^{2+}$, Dy^{3+} displayed typical NIR emission peaking at 690 nm, which was attributed to the $^4T \rightarrow {}^6A_1$ transition of Mn^{2+}.[10] In 2011, Bessière *et al.* reported the $ZnGa_2O_4:Cr^{3+}$ phosphors with persistent luminescence peaking at 695 nm for the first time.[91] Later, Pan *et al.* published an article that paved path-breaking directions in this field by proposing an innovative composition of $Zn_3Ga_2Ge_2O_{10}:Cr^{3+}$ in 2012,[36] which achieved a super-long NIR decay time of 360 h (Fig. 9A). This shockwave encouraged researchers to search for different hosts and emitters to achieve remarkable NIR persistent luminescence. Pan *et al.* also developed the NIR-emitting $LiGa_5O_8:Cr^{3+}$ with a decay time of more than 1000 h.[83] Qiu *et al.* further carried out the work of improving the persistent luminescence in $ZnGa_2O_4:Cr^{3+}$ by partially substituting Ga with Zn and Sn to form a Zn–Ga–Sn–O solid solution.[21] $Zn_3Ga_2SnO_8:Cr^{3+}$ exhibited strong and long persistent luminescence in the NIR region. Viana *et al.* systematically studied the persistent luminescence in the Cr^{3+}-doped AB_2O_4 system (A = Zn, Mg and B = Ga, Al).[92] They found that this system exhibits persistent luminescence at about 700 nm with trap depths located at about 1 eV. These traps are stable at room temperature but can be emptied by photostimulation. It is usually observed that the substituted structures of $ZnGa_2O_4:Cr^{3+}$ are more efficient in terms of both the persistent luminescence intensity and decay time.[20] Many other excellent works have also reported novel persistent phosphors featuring durable persistent luminescence in the NIR-I window.[93–98]

Compared with the NIR-I window, NIR-II and NIR-III windows show a much lower scattering coefficient, which can lead to improved resolution and deeper tissue penetration.[90] In recent years, some pioneering studies have been conducted to develop phosphors with persistent luminescence in the NIR-II and NIR-III windows.[99] Qiu *et al.* proposed a bridging cascaded energy transfer channel between Cr^{3+} and Nd^{3+} to activate persistent luminescence in the NIR-II window (Fig. 9B).[22] Based on this principle, they developed a novel $Zn_{1-x}Ca_xGa_2O_4:Cr^{3+},Nd^{3+}$ persistent phosphor with emission peaking at around 1064 nm. Tanabe *et al.* reported a persistent phosphor of $Y_3Al_2Ga_3O_{12}:Nd^{3+},Ce^{3+},Cr^{3+}$ with a long decay time at multiple wavelengths (880, 1064 and 1335 nm). The persistent luminescence covers the NIR-I and NIR-II windows,[100] which is beneficial for the preparation of multifunctional bioimaging probes. Pan *et al.* developed a novel Er^{3+} co-doped $SrAl_2O_4:Eu^{2+},Dy^{3+}$ persistent phosphor to enable energy transfer from Eu^{2+} to Er^{3+}.[101] They obtained strong persistent luminescence in the NIR-III window (around 1530 nm) with a decay time of more than 10 min (Fig. 9C). By producing persistent energy transfer from Ce^{3+} to Er^{3+}, Tanabe *et al.* have successfully developed a novel persistent phosphor $Y_3Al_2Ga_3O_{12}:Er^{3+},Ce^{3+},Cr^{3+}$ with long persistent luminescence (>10 h) in the region of 1450–1670 nm (Fig. 9D).[102] The above mentioned persistent phosphors with emissions in the NIR-II and NIR-III windows hold great potential in high resolution deep tissue bioimaging.

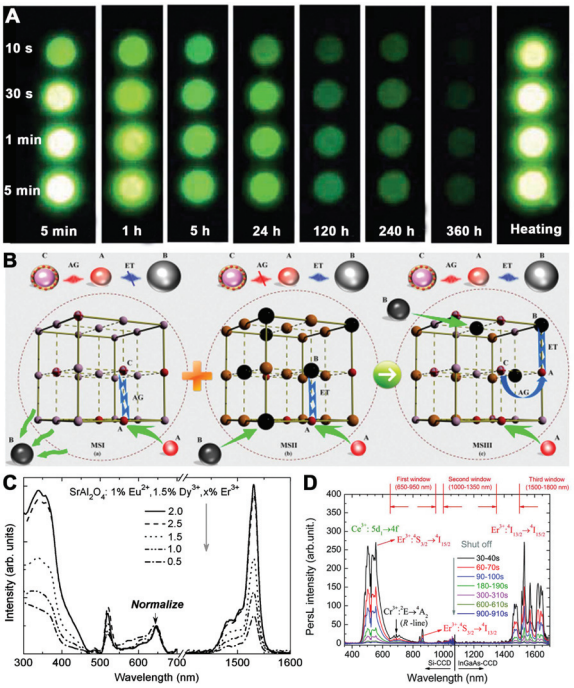

Fig. 9 (A) NIR images of four $Zn_3Ga_2Ge_2O_{10}:Cr^{3+}$ persistent phosphor discs taken at different times after irradiation by a 365 nm lamp for 10 s to 5 min. The discs were further heated at 400 °C to release the remaining charge carriers. (Reprinted with permission from ref. 36. Copyright 2012 Nature Publishing Group.) (B) Schematic illustration showing the influence of the ion doping-pattern and network-structural motifs on the energy transfer process between traps and dopants. (Reprinted with permission from ref. 22. Copyright 2016 Nature Publishing Group.) (C) NIR excitation and emission spectra of the $SrAl_2O_4:Eu^{2+},Dy^{3+}$ persistent phosphor. (Reprinted with permission from ref. 101. Copyright 2010 AIP Publishing LLC.) (D) Persistent luminescence spectra of the $Y_3Al_2Ga_3O_{12}:Nd^{3+},Ce^{3+},Cr^{3+}$ phosphor after ceasing the blue light illumination. (Reprinted with permission from ref. 102. Copyright 2016 Royal Society of Chemistry.)

5.5 Multimodal bioimaging with hybrid PLNPs

As every specific bioimaging technique (luminescence imaging, magnetic resonance imaging (MRI), computed tomography (CT)) has its own special advantages and certain constraints, multimodal bioimaging is thus proposed to obtain more precise, complete, and dependable information.[103,104] This section focuses on multimodal bioimaging based on hybrid PLNPs.

Luminescence imaging features high sensitivity and modest spatial resolution, while MRI shows high spatial resolution but moderate sensitivity.[103] Therefore, many studies have been conducted to combine luminescence imaging with MRI based on PLNPs to achieve both high sensitivity and a high spatial resolution. In 2014, Yan *et al.* put forward the idea to develop a novel multimodal bioimaging probe based on gadolinium complex-functionalized $Zn_{2.94}Ga_{1.96}Ge_2O_{10}:Cr^{3+}$, Pr^{3+} PLNPs for *in vivo* NIR luminescence imaging and MRI (Fig. 10A).[105] The probe not only possesses super long NIR persistent luminescence, but also has a relatively higher longitudinal relaxivity over the commercial gadolinium complexes. The persistent luminescence is excellent for high imaging sensitivity, while its limitation of poor spatial resolution can be readily complemented by MRI. The authors successfully utilized this novel probe for *in vivo* luminescence imaging and *T*1-weighted MRI. Doan and Richard *et al.* developed novel gadolinium-doped $ZnGa_2O_4:Cr^{3+}$ PLNPs as a versatile probe for multimodal *in vivo* bioimaging.[106] The authors showed that the probe not only allowed real-time luminescence imaging through living tissues with high sensitivity, but also allowed MRI with a high spatial resolution. The same group further reported an innovative bioimaging probe by embedding $ZnGa_2O_4:Cr^{3+}$ PLNPs and superparamagnetic iron oxide nanoparticles into mesoporous silica.[107] In addition to high imaging sensitivity and resolution, the *in vivo* motion of this probe can be guided with a magnet, which opened perspectives for applications such as targeted tumor imaging. Other excellent dual-modal bioimaging probes based on hybrid PLNPs combining luminescence imaging and MRI have also been developed, such as Gd_2O_3@$mSiO_2$@$CaTiO_3:Pr^{3+}$,[53] Gd_2O_3@$mSiO_2$/$ZnGa_2O_4:Cr^{3+}$,Bi^{3+},[54] and $Gd_2O_2S:Eu^{3+}$,Ti^{4+}, Mg^{2+}.[108]

In addition to the above dual-modal bioimaging, Wang *et al.* recently developed a novel tri-modal bioimaging probe based on $GdAlO_3:Mn^{4+}$,Ge^{4+}@Au core–shell structured PLNPs.[109] The fabrication of the multifunctional probe is illustrated in Fig. 10B. The silica shell is coated on the surface of $GdAlO_3:Mn^{4+}$,Ge^{4+} followed by gold shell growth. In the core–shell PLNPs, the $GdAlO_3:Mn^{4+}$,Ge^{4+} core serves as the NIR persistent luminescence center, and the gold shell is employed to enhance the persistent luminescence efficiency *via* plasmon resonance. The Gd element in the PLNPs can afford MRI, and the Au element can provide CT. *In vivo* bioimaging results demonstrate that each modality of the probe is comparable or superior to the previously reported probes, making this probe valuable in applications such as disease diagnosis and monitoring the biological processes.

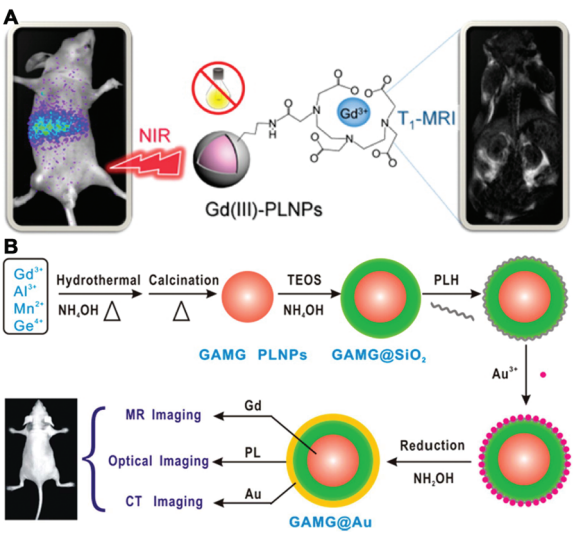

Fig. 10 (A) Schematic illustration of luminescence imaging and MRI based on gadolinium complex-functionalized $Zn_{2.94}Ga_{1.96}Ge_2O_{10}:Cr^{3+}$, Pr^{3+} PLNPs. (Reprinted with permission from ref. 105. Copyright 2014 American Chemical Society.) (B) Schematic illustration of the preparation of the $GdAlO_3:Mn^{4+}$,Ge^{4+}@Au PLNP-based probe for *in vivo* tri-modal bioimaging. (Reprinted with permission from ref. 109. Copyright 2016 American Chemical Society.)

6. Imaging-guided therapy based on PLNPs

The growing demand for advanced cancer diagnosis and therapy has led to the construction of a biomedicine system that integrates bioimaging and therapy into a single nanoplatform for imaging-guided cancer therapy, which can achieve higher therapeutic efficiency and less side effects.[110] A bioimaging probe, which is one of the most important parts of the theranostic system, is responsible for identifying the location of cancer tissue, monitoring the biodistribution of the nanoplatforms and assessing the therapeutic efficacy.[19] Considering the special advantages of PLNPs in bioimaging, an important area will be developed by integrating PLNPs with other functional materials (such as photo-thermal nanomaterials) to open doors to novel imaging-guided therapy in the fields of biomedicine.

6.1 Imaging-guided chemotherapy

Chemotherapy drug delivery has attracted enormous attention in the past few decades due to its great promise in eliminating side effects and improving therapeutic efficiency.[111–113] Imaging-guided chemotherapy can help to understand the state of the drugs after *in vivo* administration.[110] The bioimaging probe based on PLNPs features superior sensitivity and a high SNR, making it ideal for monitoring the location of drugs and guiding the subsequent cancer therapy. The appli-

cations of PLNPs in imaging-guided chemotherapy have been explored in the past few years.

Taking advantage of the high pore volume of mesoporous silica and the durable NIR persistent luminescence in $ZnGa_2O_4:Cr^{3+}$ PLNPs, Richard *et al.* developed novel $ZnGa_2O_4$:Cr@mSiO_2 PLNPs for both highly sensitive bioimaging and concomitant drug delivery (Fig. 11A).[114] The authors demonstrated that the mesoporous hybrid PLNPs could efficiently load an anticancer agent, and subsequently release the drug in a pH-sensitive manner. The doxorubicin-loaded theranostic agent showed acute cytotoxicity toward U87MG cells. Moreover, the biodistribution of the drug-loaded probe could be easily monitored *in vivo*, providing valuable information about the localization of the major drug-release area.

The MSNs are widely used in biomedicine, such as drug delivery and bioimaging due to their easy preparation and good biocompatibility. As we introduced in section 3, Zhang *et al.* have made a great contribution in the preparation of PLNPs by using MSNs as the template. The MSNs can not only serve as the template to control the growth of PLNPs, but also can be used as a drug carrier. Zhang and coworkers have also developed a series of imaging-guided chemotherapy systems by using MSNs as both drug carriers and morphology-controlling templates. For instance, they prepared a kind of SiO_2/$Zn_{1.1}Ga_{1.8}Ge_{0.1}O_4:Cr^{3+},Eu^{3+}$ for both tumor targeted imaging and drug delivery.[52] The hybrid PLNPs were prepared using the template method, and the obtained hybrid PLNPs were functionalized with folic acid for the targeted recognition of cancer cells. The anticancer drugs can be further loaded into the pores of the mesoporous silica. The obtained PLNPs showed a large pore capacity and bright NIR persistent luminescence lasting for 15 days. The authors demonstrated that the developed PLNPs showed efficient drug release and excellent tumor targeting ability with high sensitivity both *in vitro* and *in vivo*. Recently, a novel multimodal imaging-guided chemotherapy system has been developed based on the Gd_2O_3@mSiO_2/$ZnGa_2O_4:Cr^{3+}$ PLNPs.[54] The authors showed that the drug release process was overall slow and about 99% of doxorubicin was released after 65 h, suggesting the potential application of the PLNPs in the construction of a controlled or delayed drug delivery system. Moreover, the PLNPs also exhibited high sensitivity and spatial resolution in targeted tumor imaging.

6.2 Imaging-guided photothermal therapy

Photothermal therapy (PTT) is an effective cancer treatment method and has been used with increasing frequency. The PTT usually causes little long term side effects and can be repeated many times to achieve high therapeutic efficiency.[115] Optical imaging can provide accurate information about the location and area of tumor tissue for highly specific PTT.

Recently, Wang *et al.* developed a novel persistent luminescence imaging-guided PTT system by co-loading photothermal therapy agents and PLNPs into mesoporous silica nanocarriers.[23] As illustrated in Fig. 12, $CaZnTiO_3:Pr^{3+}$ PLNPs are coated with a mesoporous silica shell, and the photothermal therapy agent indocyanine green (ICG) is further loaded into the mesoporous shell. The PLNPs can be pre-charged and further used for tracking the nanoplatform *in vivo*, while the ICG can be repeatedly activated with 808 nm light for efficient PTT. The authors demonstrated that the PTT probe exhibited a high SNR during *in vivo* luminescence imaging-guided PTT. Moreover, mice treated with the PTT probe showed significantly inhibited tumor growth.

6.3 Imaging-guided photodynamic therapy

The basic mechanism of photodynamic therapy (PDT) is using a photosensitizer along with light to generate a cytotoxic singlet oxygen ($^1O_2$) to kill cancer cells. PDT is a potential alternative to conventional cancer therapeutic methods owing to its highly spatial and temporal control of the therapy process.[107] However, continuous light irradiation is needed in traditional PDT to activate the photosensitizers. The therapy efficiency may be compromised by the limited penetration depth of visible excitation sources.[116] Moreover, possible side effects such as overheating and cell damage have also been

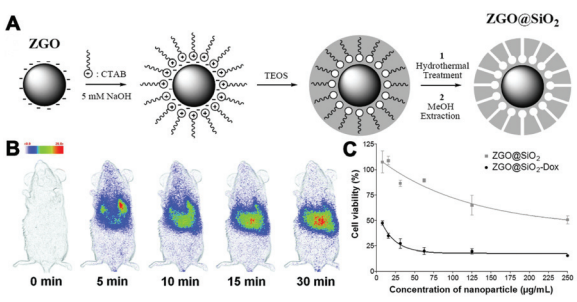

Fig. 11 (A) Schematic representation of the preparation of $ZnGa_2O_4$:Cr@mSiO_2 PLNPs. (B) *In vivo* biodistribution of the PLNP-based probe in a mouse after intravenous injection. (C) Relative viability of U87MG cells after 24 h of incubation with either $ZnGa_2O_4$:Cr@mSiO_2 or Dox-loaded $ZnGa_2O_4$:Cr@mSiO_2. (Reprinted with permission from ref. 114. Copyright 2014 Royal Society of Chemistry.)

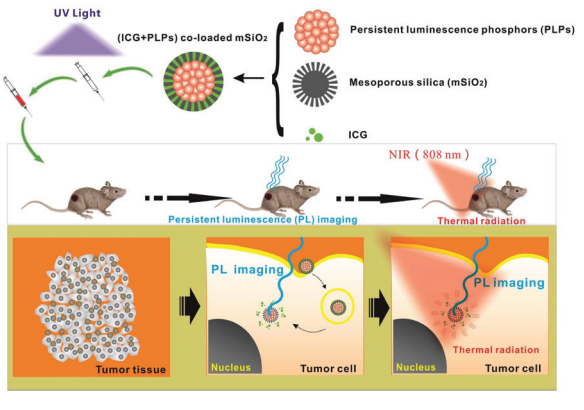

Fig. 12 Schematic representation of the applications of $CaZnTiO_3:Pr^{3+}$ hybrid PLNPs for persistent luminescence imaging-guided PTT *in vivo*. (Reprinted with permission from ref. 23. Copyright 2016 American Chemical Society.)

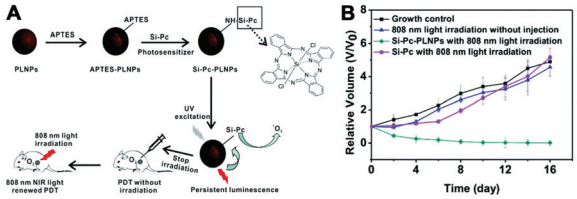

Fig. 13 (A) Schematic illustration for the design of the persistent luminescence sensitized PDT platform. (B) *In vivo* photodynamic therapy efficiency. (Reprinted with permission from ref. 24. Copyright 2016 Royal Society of Chemistry.)

concerned from *in situ* irradiation with NIR excitation sources.[117] The PLNPs hold great potential to solve such problems because they can continuously activate the photosensitizers with persistent energy, that is, continuous light irradiation is not required.

Very recently, Yan *et al.* reported the conjugation of a NIR-absorbing photosensitizer to $Zn_3Ga_4Ge_2O_{13}:Cr^{3+}$ PLNPs for renewable persistent luminescence sensitized PDTs without any need for continuous light irradiation.[24] Their design is outlined in Fig. 13A. (3-Amino propyl)triethoxysilane was utilized to introduce an amino group into the surface of PLNPs, and photosensitizer Si-Pc was further covalently linked to PLNPs to construct the PDT probe. The probe was pre-charged with UV light and then injected into the tumor tissue for PDT. The overlap between the emission band of the PLNPs and the absorption band of the photosensitizer Si-Pc provides the foundation for the generation of $^1O_2$ with persistent luminescence activation. Moreover, the persistent luminescence can be efficiently recovered with 808 nm light stimulation. The authors demonstrated that the tumor volume in mice injected with the pre-excited Si-Pc-PLNPs and stimulated with 808 nm light significantly decreased over time, showing the effective persistent luminescence sensitized *in vivo* PDT (Fig. 13B). In addition, the nanoplatform and 808 nm NIR light stimulation showed no obvious damage to the normal organs of the mice, showing greatly reduced side effects.

7. Conclusions and prospects

Persistent phosphors, a novel luminescent material with a super-long decay time, have attracted a wide range of attention in biomedicine. In this review, we discussed the recent developments in the preparation of PLNPs and the applications of PLNPs in biosensing, bioimaging and cancer therapy. Persistent phosphors possess a special advantage in eliminating autofluorescence interference since *in situ* excitation is not required, and they are ideal for long-term bioimaging due to their super-long decay time. In order to promote the biomedical applications of persistent phosphors, many top-down and bottom-up methods have been developed for the preparation of PLNPs. Several pioneering works on exploring the biosensing application of PLNPs have been conducted, and a superior SNR has been achieved in analyzing biomolecules in complicated biological samples. Different kinds of PLNPs have been rationally designed in the past decade to enhance the persistent luminescence intensity and increase the decay time to achieve better *in vivo* imaging performance. Compared to bioimaging, the application of PLNPs in therapy is still in its early stage. Persistent luminescence imaging-guided therapy can afford visualized cancer therapy with a high SNR. Moreover, the possible overheating and tissue damage associated with continuous *in situ* external excitation in traditional photo-assisted therapy can also be efficiently reduced. In a word, PLNPs show unprecedented advantages in biosensing, bioimaging and cancer therapy.

Acknowledgements

This work was supported by the National Natural Science Foundation of China (21422105, 21675120) and the Ten Thousand Talents Program for Young Talents.

References

1 Y. Li, M. Gecevicius and J. Qiu, *Chem. Soc. Rev.*, 2016, **45**, 2090–2136.
2 T. Matsuzawa, Y. Aoki, N. Takeuchi and Y. Murayama, *J. Electrochem. Soc.*, 1996, **143**, 2670–2673.
3 K. Van den Eeckhout, P. F. Smet and D. Poelman, *Materials*, 2010, **3**, 2536–2566.
4 C. Zirkle, *Isis*, 1959, **50**, 68–69.
5 P. F. Smet, I. Moreels, Z. Hens and D. Poelman, *Materials*, 2010, **3**, 2834–2883.
6 P. F. Smet, J. Botterman, K. V. D. Eeckhout, K. Korthout and D. Poelman, *Opt. Mater.*, 2014, **36**, 1913–1919.
7 K. V. D. Eeckhout, D. Poelman and P. F. Smet, *Materials*, 2013, **6**, 2789–2818.
8 Y. Wang, Y. Gong, X. Xu and Y. Li, *J. Lumin.*, 2013, **133**, 25–29.
9 J. T. Kong, W. Zheng, Y. S. Liu, R. F. Li, E. Ma, H. M. Zhu and X. Y. Chen, *Nanoscale*, 2015, **7**, 11048–11054.
10 Q. M. de Chermont, C. Chanéac, J. Seguin, F. Pellé, S. Maîtrejean, J. P. Jolivet, D. Gourier, M. Bessodes and D. Scherman, *Proc. Natl. Acad. Sci. U. S. A.*, 2007, **104**, 9266–9271.
11 T. Maldiney, A. Bessière, J. Seguin, E. Teston, S. K. Sharma, B. Viana, A. J. J. Bos, P. Dorenbos, M. Bessodes, D. Gourier, D. Scherman and C. Richard, *Nat. Mater.*, 2014, **13**, 418–426.
12 Y. Zhuang, Y. Katayama, J. Ueda and S. Tanabe, *Opt. Mater.*, 2014, **36**, 1907–1912.
13 L. Song, X. H. Lin, X. R. Song, S. Chen, X. F. Chen, J. Li and H. H. Yang, *Nanoscale*, 2017, **9**, 2718–2722.
14 T. Maldiney, A. Lecointre, B. Viana, Al. Bessière, M. Bessodes, D. Gourier, C. Richard and D. Scherman, *J. Am. Chem. Soc.*, 2011, **133**, 11810–11815.

15 A. Abdukayum, J. T. Chen, Q. Zhao and X. P. Yan, *J. Am. Chem. Soc.*, 2013, **135**, 14125–14133.
16 T. Maldiney, C. Richard, J. Seguin, N. Wattier, M. Bessodes and D. Scherman, *ACS Nano*, 2011, **5**, 854–862.
17 Z. J. Li, Y. W. Zhang, X. Wu, X. Q. Wu, R. Maudgal, H. W. Zhang and G. Han, *Adv. Sci.*, 2015, **2**, 1500001.
18 Z. Li, Y. Zhang, X. Wu, L. Huang, D. Li, W. Fan and G. Han, *J. Am. Chem. Soc.*, 2015, **137**, 5304–5307.
19 J. Yu, C. Yang, J. Li, Y. Ding, L. Zhang, M. Z. Yousaf, J Lin, R. Pang, L. B. Wei, L. L. Xu, F. G. Sheng, C. H. Li, G. J. Li, L. Y. Zhao and Y. L. Hou, *Adv. Mater.*, 2014, **26**, 4114–4120.
20 M. Allix, Sb. Chenu, E. Véron, T. Poumeyrol, E. A. Kouadri-boudjelthia, S. Alahrache, F. Porcher, D. Massiot and F. Fayon, *Chem. Mater.*, 2013, **25**, 1600–1606.
21 Y. Li, S. Zhou, Y. Li, K. Sharafudeen, Z. Ma, G. Dong, M. Y. Peng and J. R. Qiu, *J. Mater. Chem. C*, 2014, **2**, 2657–2663.
22 X. Qin, Y. Li, R. Zhang, J. Ren, M. Gecevicius, Y. Wu, K. Sharafudeen, G. P. Dong, S. F. Zhou, Z. J. Ma and J. R. Qiu, *Sci. Rep.*, 2016, **6**, 20275.
23 B. Zheng, H. Chen, P. Zhao, H. Pan, X. Wu, X. Gong, H. J. Wang and J. Chang, *ACS Appl. Mater. Interfaces*, 2016, **8**, 21603–21611.
24 R. Abdurahman, C. X. Yang and X. P. Yan, *Chem. Commun.*, 2016, **52**, 13303–13306.
25 B. Viana, S. K. Sharma, D. Gourier, T. Maldiney, E. Teston, D. Scherman and C. Richard, *J. Lumin.*, 2016, **170**, 879–887.
26 T. Lécuyer, E. Teston, G. Ramirez-Garcia, T. Maldiney, B. Viana, J. Seguin, N. Mignet, D. Scherman and C. Richard, *Theranostics*, 2016, **6**, 2488–2524.
27 H. F. Brito, J. Hölsä, T. Laamanen, M. Lastusaari, M. Malkamäki and L. C. Rodrigues, *Opt. Mater. Express*, 2012, **2**, 371–381.
28 F. Wang, B. Yang, D. Liu, W. Ma, X. Chen and Y. Dai, *Spectrochim. Acta, Part A*, 2014, **126**, 46–52.
29 L. C. V. Rodrigues, H. F. Brito, J. Hölsä, R. Stefani, M. C. F. C. Felinto, M. Lastusaari, T. Laamanen and L. A. O. Nunes, *J. Phys. Chem. C*, 2012, **116**, 11232–11240.
30 B. Qu, B. Zhang, L. Wang, R. Zhou, X. C. Zeng and L. Li, *ACS Appl. Mater. Interfaces*, 2016, **8**, 5439–5444.
31 Y. Li, S. Zhou, G. Dong, M. Peng, L. Wondraczek and J. R. Qiu, *Sci. Rep.*, 2014, **4**, 4059.
32 Y. Zhuang, J. Ueda and S. Tanabe, *J. Mater. Chem. C*, 2013, **1**, 7849–7855.
33 M. Sun, Z. J. Li, C. L. Liu, H. X. Fu, J. S. Shen and H. W. Zhang, *J. Lumin.*, 2014, **145**, 838–842.
34 B. B. Srivastava, A. Kuang and Y. Mao, *Chem. Commun.*, 2015, **51**, 7372–7375.
35 E. Teston, S. Richard, T. Maldiney, N. Lièvre, G. Y. Wang, L. Motte, C. Richard and Y. Lalatonne, *Chem. – Eur. J.*, 2015, **21**, 7350–7354.
36 Z. Pan, Y. Y. Lu and F. Liu, *Nat. Mater.*, 2012, **11**, 58–63.
37 T. Maldiney, B. Viana, A. Bessière, D. Gourier, M. Bessodes, D. Scherman and C. Richard, *Opt. Mater.*, 2013, **35**, 1852–1858.
38 B. Y. Wu, H. F. Wang, J. T. Chen and X. P. Yan, *J. Am. Chem. Soc.*, 2011, **133**, 686–688.
39 X. Fu, C. Liu, J. Shi, H. Man, J. Xu and H. Zhang, *Opt. Mater.*, 2014, **36**, 1792–1797.
40 C. Rosticher, B. Viana, T. Maldiney, C. Richard and C. Chanéac, *J. Lumin.*, 2016, **170**, 460–466.
41 T. Maldiney, G. Sraiki, B. Viana, D. Gourier, C. Richard, D. Scherman, M. Bessodes, K. Van den Eeckhout, D. Poelman and P. F. Smet, *Opt. Mater. Express*, 2012, **2**, 261–268.
42 Z. J. Li, H. W. Zhang, M. Sun, J. S. Shen and H. X. Fu, *J. Mater. Chem.*, 2012, **22**, 24713–24720.
43 X. C. Jiang, C. H. Yan, L. D. Sun, Z. G. Wei and C. S. Liao, *J. Solid State Chem.*, 2003, **175**, 245–251.
44 C. Li, J. Yang, P. Yang, H. Lian and J. Lin, *Chem. Mater.*, 2008, **20**, 4317–4326.
45 C. Li, J. Yang, Z. Quan, P. Yang, A. Deyan Kong and J. Lin, *Chem. Mater.*, 2007, **19**, 4933–4942.
46 J. Shi, X. Sun, J. Zhu, J. Li and H. Zhang, *Nanoscale*, 2016, **8**, 9798–9804.
47 A. Mondal, S. Das and J. Manam, *RSC Adv.*, 2016, **6**, 82484–82495.
48 Z. Li, J. Shi, H. Zhang and M. Sun, *Opt. Express*, 2014, **22**, 10509–10518.
49 S. Das, J. Manam and S. K. Sharma, *ECS J. Solid State Sci. Technol.*, 2016, **5**, R98–R103.
50 J. Tang, Y. Su, D. Deng, L. Zhang, N. Yang and Y. Lv, *Analyst*, 2016, **141**, 5366–5373.
51 Z. J. Li, Y. J. Zhang, H. W. Zhang and H. X. Fu, *Microporous Mesoporous Mater.*, 2013, **176**, 48–54.
52 J. Shi, X. Sun, J. Li, H. Man, J. Shen, Y. Yu and H. W. Zhang, *Biomaterials*, 2015, **37**, 260–270.
53 J. P. Shi, H. X. Fu, X. Sun, J. S. Shen and H. W. Zhang, *J. Mater. Chem. B*, 2015, **3**, 635–641.
54 W. B. Dai, Y. F. Lei, S. Ye, E. H. Song, Z. Chen and Q. Y. Zhang, *J. Mater. Chem. B*, 2016, **4**, 1842–1852.
55 Y. F. Xu, D. K. Ma, M. L. Guan, X. A. Chen, Q. Q. Pan and S. M. Huang, *J. Alloys Compd.*, 2010, **502**, 38–42.
56 B. Cheng, L. Fang, Z. Zhang, Y. Xiao and S. Lei, *J. Phys. Chem. C*, 2011, **115**, 1708–1713.
57 D. Liu, C. E. Cui, P. Huang, L. Wang and G. Jiang, *J. Alloys Compd.*, 2014, **583**, 530–534.
58 W. Li, Y. Liu and P. Ai, *Mater. Chem. Phys.*, 2010, **119**, 52–56.
59 W. Zheng, D. T. Tu, P. Huang, S. Y. Zhou, Z. Chen and X. Y. Chen, *Chem. Commun.*, 2015, **51**, 4129–4143.
60 B. Zhou, B. Y. Shi, D. Y. Jin and X. G. Liu, *Nat. Nanotechnol.*, 2015, **10**, 924–936.
61 W. Zheng, P. Huang, D. T. Tu, E. Ma, H. M. Zhu and X. Y. Chen, *Chem. Soc. Rev.*, 2015, **44**, 1379–1415.
62 P. Huang, W. Zheng, S. Y. Zhou, D. T. Tu, Z. Chen, H. M. Zhu, R. F. Li, E. Ma, M. D. Huang and X. Y. Chen, *Angew. Chem., Int. Ed.*, 2014, **53**, 1252–1257.

63 W. Zheng, S. Y. Zhou, J. Xu, Y. S. Liu, P. Huang, Y. Liu and X. Y. Chen, *Adv. Sci.*, 2016, **3**, 1600197.
64 K. Shiraki, K. Takase, Y. Tameda, M. Hamada, Y. Kosaka and T. Nakano, *Hepatology*, 1995, **22**, 802–807.
65 N. Li, Y. Li, Y. Han, W. Pan, T. Zhang and B. Tang, *Anal. Chem.*, 2014, **86**, 3924–3930.
66 N. Li, W. Diao, Y. Han, W. Pan, T. Zhang and B. Tang, *Chem. – Eur. J.*, 2014, **20**, 16488–16491.
67 L. Zhang, J. Lei, J. Liu, F. Ma and H. Ju, *Biomaterials*, 2015, **67**, 323–334.
68 Y. Tang, H. Song, Y. Su and Y. Lv, *Anal. Chem.*, 2013, **85**, 1876–11884.
69 A. S. Paterson, B. Raja, G. Garvey, A. Kolhatkar, A. E. Hagström, K. Kourentzi, T. R. Lee and R. C. Willson, *Anal. Chem.*, 2014, **86**, 9481–9488.
70 R. J. Cooper, *Nat. Photonics*, 2014, **8**, 425–426.
71 J. Zhou, Z. Liu and F. Li, *Chem. Soc. Rev.*, 2012, **41**, 1323–1349.
72 Y. He, Y. Zhong, Y. Su, Y. Lu, Z. Jiang, F. Peng, T. Xu, S. Su, Q. Huang, C. H. Fan and S.-T. Lee, *Angew. Chem., Int. Ed.*, 2011, **50**, 5695–5698.
73 D. Ling, M. J. Hackett and T. Hyeon, *Nat. Mater.*, 2014, **13**, 122–124.
74 G. Han and G. Chen, *Theranostics*, 2013, **3**, 354–355.
75 H. Xu, Q. Li, L. Wang, Y. He, J. Shi, B. Tang and C. Fan, *Chem. Soc. Rev.*, 2014, **43**, 2650–2661.
76 T. Maldiney, M. U. Kaikkonen, J. Seguin, Q. le Masne de Chermont, M. Bessodes, K. J. Airenne, S. Ylä-herttuala, D. Scherman and C. Richard, *Bioconjugate Chem.*, 2012, **23**, 472–478.
77 T. Maldiney, G. Byk, N. Wattier, J. Seguin, R. Khandadash, M. Bessodes, C. Richard and D. Scherman, *Int. J. Pharm.*, 2012, **423**, 102–107.
78 A. Bessière, S. K. Sharma, N. Basavaraju, K. R. Priolkar, L. Binet, B. Viana, J. J. Adriebos, T. Maldiney, C. Richard, D. Scherman and D. Gourier, *Chem. Mater.*, 2014, **26**, 1365–1373.
79 D. Gourier, A. Bessière, S. K. Sharma, L. Binet, B. Viana, N. Basavaraju and K. R. Priolkarb, *J. Phys. Chem. Solids*, 2014, **75**, 826–837.
80 S. Q. Wu, C. W. Chi, C. X. Yang and X. P. Yan, *Anal. Chem.*, 2016, **88**, 4114–4121.
81 S. K. Sharma, D. Gourier, E. Teston, D. Scherman, C. Richard and B. Viana, *Opt. Mater.*, 2017, **63**, 51–58.
82 D. C. R. Burbano, S. K. Sharma, P. Dorenbos, B. Viana and J. A. Capobianco, *Adv. Opt. Mater.*, 2015, **3**, 551–557.
83 F. Liu, W. Yan, Y. J. Chuang, Z. Zhen, J. Xie and Z. Pan, *Sci. Rep.*, 2013, **3**, 1554.
84 Y. J. Chuang, Z. Zhen, F. Zhang, F. Liu, J. P. Mishra, W. Tang, H. H. Chen, X. L. Huang, L. C. Wang, X. Y. Chen, J. Xie and Z. W. Pan, *Theranostics*, 2014, **4**, 1112–1122.
85 D. C. R. Burbano, E. M. Rodríguez, P. Dorenbos, M. Bettinelli and J. A. Capobianco, *J. Mater. Chem. C*, 2014, **2**, 228–231.
86 B. Zhang, X. Yu, T. Wang, S. Cheng, J. Qiu and X. Xu, *J. Am. Ceram. Soc.*, 2015, **98**, 171–177.
87 B. Zhang, X. Xu, Q. Li, Y. Wu, J. Qiu and X. Yu, *J. Solid State Chem.*, 2014, **217**, 136–141.
88 E. Hemmer, N. Venkatachalam, H. Hyodo, A. Hattori, Y. Ebina, H. Kishimoto and K. Sogam, *Nanoscale*, 2013, **5**, 11339–11361.
89 J. C. G. Bünzli, *J. Lumin.*, 2016, **170**, 866–878.
90 A. M. Smith, M. C. Mancini and S. Nie, *Nat. Nanotechnol.*, 2009, **4**, 710–711.
91 A. Bessière, S. Jacquart, K. Priolkar, A. Lecointre, B. Viana and D. Gourier, *Opt. Express*, 2011, **19**, 10131–10137.
92 S. K. Sharma, D. Gourier, B. Viana, T. Maldiney, E. Teston, D. Scherman and C. Richard, *Opt. Mater.*, 2014, **36**, 1901–1906.
93 Y. Katayama, H. Kobayashi and S. Tanabe, *Appl. Phys. Express*, 2014, **8**, 012102.
94 W. Chen, Y. Wang, W. Zeng, G. Li and H. Guo, *RSC Adv.*, 2015, **6**, 331–337.
95 F. Sun, R. Xie, L. Guan and C. Zhang, *Mater. Lett.*, 2016, **164**, 39–43.
96 Y. Li, Y. Y. Li, K. Sharafudeen, G. P. Dong, S. F. Zhou, Z. J. Ma, M. Y. Peng and J. R. Qiu, *J. Mater. Chem. C*, 2013, **2**, 2019–2027.
97 R. Pang, Y. Jia, R. Zhao, H. Li, J. Fu, W. Sun, L. H. Jiang, S. Zhang, C. Y. Li and Q. Su, *Dalton Trans.*, 2014, **43**, 9661–9668.
98 J. Xu, J. Ueda, Y. Zhuang, B. Viana and S. Tanabe, *Appl. Phys. Express*, 2015, **8**, 042602.
99 S. Kamimura, C. N. Xu, H. Yamada, N. Terasaki and M. Fujihala, *Jpn. J. Appl. Phys.*, 2014, **53**, 092403.
100 J. Xu, S. Tanabe, A. D. Sontakke and J. Ueda, *Appl. Phys. Lett.*, 2015, **107**, 081903.
101 N. Yu, F. Liu, X. Li and Z. Pan, *Appl. Phys. Lett.*, 2010, **95**, 231110.
102 J. Xu, D. Murata, J. Ueda and S. Tanabe, *J. Mater. Chem. C*, 2016, **4**, 11096–11103.
103 N. Erathodiyil and J. Y. Ying, *Acc. Chem. Res.*, 2011, **44**, 9925–9935.
104 P. Sharma, S. Brown, G. Walter, S. Santra and B. Moudgil, *Adv. Colloid Interface Sci.*, 2006, **123**, 471–485.
105 A. Abdukayum, C. X. Yang, Q. Zhao, J. T. Chen, L. X. Dong and X. P. Yan, *Anal. Chem.*, 2014, **86**, 4096–4101.
106 T. Maldiney, B. T. Doan, D. Alloyeau, M. Bessodes, D. Scherman and C. Richard, *Adv. Funct. Mater.*, 2015, **25**, 331–338.
107 E. Teston, Y. Lalatonne, D. Elgrabli, G. Autret, L. Motte, F. Gazeau, D. Scherman, O. Clément, C. Richard and T. Maldiney, *Small*, 2015, **11**, 2696–2704.
108 C. Chaneac, C. Rosticher, B. Viana, M. A. Fortin, J. Lagueux and L. Faucher, *RSC Adv.*, 2016, **6**, 55472–55478.
109 J. M. Liu, Y. Y. Liu, D. D. Zhang, G. Fang and S. Wang, *ACS Appl. Mater. Interfaces*, 2016, **8**, 29939–29949.
110 H. Ding and F. Wu, *Theranostics*, 2012, **2**, 1037–1039.

111 P. Yang, S. Gai and J. Lin, *Chem. Soc. Rev.*, 2012, **41**, 3679–3698.
112 H. Pei, X. Zuo, D. Zhu, Q. Huang and C. Fan, *Acc. Chem. Res.*, 2014, **47**, 550–559.
113 X. Ouyang, J. Li, H. Liu, B. Zhao, J. Yan, Y. Ma, S. J. Xiao, S. P. Song, Q. Huang, J. Chao and C. H. Fan, *Small*, 2013, **9**, 3082–3087.
114 T. Maldiney, B. Ballet, M. Bessodes, D. Scherman and C. Richard, *Nanoscale*, 2014, **6**, 13970–13976.
115 S. Wang, P. Huang, L. Nie, R. Xing, D. Liu, Z. Wang, J. Lin, S. H. Chen, G. Niu, G. M. Lu and X. Y. Chen, *Adv. Mater.*, 2013, **25**, 3055–3061.
116 Q. Yuan, Y. Wu, J. Wang, D. Lu, Z. Zhao, T. Liu, X. B. Zhang and W. H. Tan, *Angew. Chem., Int. Ed.*, 2013, **52**, 13965–13969.
117 G. Yang, D. Yang, P. Yang, R. Lv, C. Li, C. Zhong, F. He, S. L. Gai and J. Lin, *Chem. Mater.*, 2015, **27**, 7957–7968.